An analysis of the gyroscope dynamics of an anti-aircraft missile launched from a mobile platform

Z. KORUBA*, I. KRZYSZTOFIK, and Z. DZIOPA

Faculty of Mechatronics and Machine Building, Kielce University of Technology
7 1000-lecia Państwa Polskiego Ave., 25-314 Kielce, Poland

Abstract. The work considers the effect of the kinematic action resulting from the basic motion of the vehicle on the dynamics of the launcher and the gyroscope acting as the drive of the opto-electro-mechanical target coordinator in a self-guided missile. The problem was analyzed using a hypothetical short-range anti-aircraft system. The simulation results were represented graphically.

Key words: missile launcher, missile rocket, gyroscope correction.

1. Introduction

The analysis was conducted for a missile equipped with a controlled mechanical gyroscope suspended on a Cardan joint [1], whose diagram is presented in Fig. 1. It is assumed that:

a) the rotor motor mass does not coincide with the centre of the inner frame mass and the motion centre, O, i.e. the point of intersection of the axis of rotation of the rotor and the frames. The considerations concerned a heavy gyroscope.

b) the Ox_1, Oy_1, Oz_1 axes are main central axes of inertia of the outer frame; in a similar way, the Ox_2, Oy_2, Oz_2 and Ox_3, Oy_3, Oz_3 axes are the main central axes of inertia of the inner frame and the rotor, respectively.

We assumed that the following quantities were known:

1. m_1, m_2, m_3 – masses of the gyroscope outer and inner frames and the rotor, respectively;
2. J_{x_1}, J_{y_1}, J_{z_1} – moments of inertia of the outer frame with regard to the Ox_1, Oy_1, and Oz_1 axes, respectively;
3. J_{x_2}, J_{y_2}, J_{z_2} – moments of inertia of the inner frame with regard to the Ox_2, Oy_2, Oz_2 axes, respectively;
4. J_{x_3}, J_{y_3}, J_{z_3} – moments of inertia of the rotor with regard to the Ox_3, Oy_3, Oz_3 axes, respectively;
5. $\overrightarrow{\omega}_p^*\,(\boldsymbol{p}^*,\, \boldsymbol{q}^*,\, \boldsymbol{r}^*)$ – components of the angular velocity vector of the platform (kinematic excitation of the platform);
6. $\overrightarrow{V}_p\,(V_p, 0,\, 0)$ – components of the linear velocity vector of the platform displacements – coordinates of velocity of point O in the system connected with the platform;
7. $\overrightarrow{F}_g\,(F_{x_3}, F_{y_3}, F_{z_3})$ – components of the force acting on the rotor mass centre given in the coordinate system connected with the platform, $Oxyz$;
8. Moments of the interaction forces: $\overrightarrow{M}_c$– between the platform and the outer frame; $\overrightarrow{M}_b$ – between the outer frame and the inner frame; $\overrightarrow{M}_k$ – between the inner frame and the rotor;

9. moments of the viscous friction forces in the bearings of the inner and outer frames $M_{rb} = \eta_b \dfrac{d\vartheta_g}{dt}$ and $M_{rc} = \eta_c \dfrac{d\psi_g}{dt}$, respectively; where: η_c, η_b, μ_c, μ_b – coefficients of friction in the bearings;

10. $\overrightarrow{M}_{rk}$ – moment of the friction forces in the bearings of the inner frame and the rotor and the aerodynamic resistances.
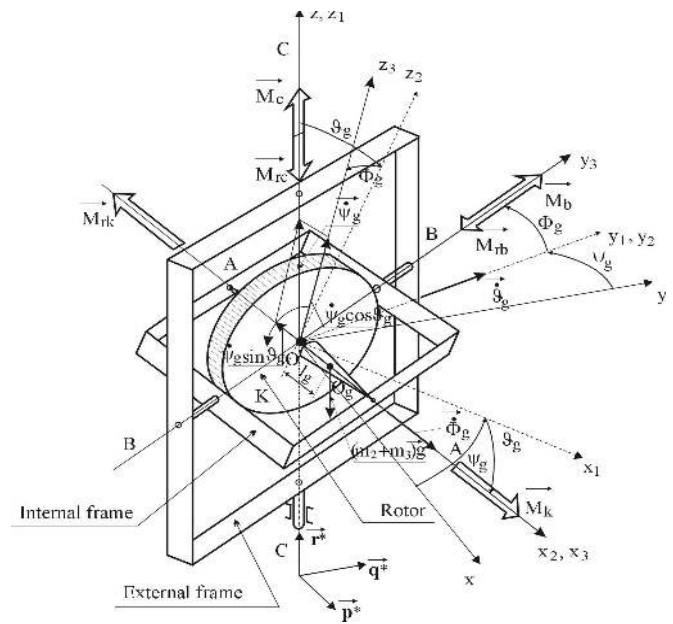

Fig. 1. General view of the gyroscope with the assumed coordinate systems after Ref. [1]

The model of the launcher-missile-gyroscope system [1] has seven degrees of freedom, which results from the structure of the formulated model. The positions of the system at any moment were determined assuming seven independent generalized coordinates:

*e-mail: ksmzko@tu.kielce.pl

1. y_v – vertical displacement of the turret mass centre, S_v;
2. φ_v – angle of rotation of the turret about the $S_v x_v$ axis;
3. ϑ_v – angle of rotation of the pedestal about the $S_v z_v$ axis;
4. ξ_{pv} – straightline displacement of the missile mass centre, S_p, along the $S_v \xi_{pv}$ axis;
5. ψ_g – angle of rotation of the gyroscope outer frame;
6. ϑ_g – angle of rotation of the gyroscope inner frame;
7. Φ_g – angle of rotation of the gyroscope rotor frame.

Equations of motion of the controlled gyroscope. It was assumed that the rotor was an axial and symmetrical body: $J_{x_3} = J_{go}$, $J_{y_3} = J_{z_3} = J_{gk}$. Moreover, when $M_k = M_{rk}$, we had $\omega_{gx_3} \approx const = n_g$. Thus, we obtained two equations describing the gyroscope motion

$$
\begin{aligned}
&\left[J_{y_2} + J_{gk} + (m_2 + m_3) \cdot l_g^2 \right] \frac{d\omega_{gy_3}}{dt} + \\
&+ (J_{x_2} - J_{z_2} - J_{gk}) \omega_{gx_2} \omega_{gz_3} + J_{go} n_g \omega_{gz_3} + \\
&+ (m_2 + m_3) \cdot l_g \left[\left(\dot{\omega}_{gy_1} l_g - V_{gx_1} \dot{\vartheta}_g \right) \cos \vartheta_g + V_{gx_2} \omega_{gy_2} + \right. \\
&\left. - V_{gy_2} \omega_{gx_2} - \left(\omega_{gy_1} \dot{\vartheta}_g l_g + \dot{V}_{gx1} \cos \vartheta_g \right) \sin \vartheta_g \right] = \\
&\quad\quad = M_b + M_g - M_{rb},
\end{aligned}
\tag{1}
$$

$$
\begin{aligned}
&\left[J_{z_2} + J_{gk} + (m_2 + m_3) \cdot l_g^2 \right] \frac{d}{dt} \left(\omega_{gz_2} \cos \vartheta_g \right) - \\
&- \left[(J_{x_2} + J_{go}) \dot{\omega}_{gx_2} + (J_{z_2} + J_{gk}) \omega_{gy_1} \omega_{gz_2} \right] \sin \vartheta_g - \\
&- (J_{x_2} \omega_{gx_2} + J_{go} n_g) \left(\omega_{gy_1} + \dot{\vartheta}_g \right) \cos \vartheta_g + \\
&+ (J_{y_2} + J_{gk}) \omega_{gy_2} \omega_{gx_1} + (J_{y_1} - J_{x_1}) \omega_{gx_1} \omega_{gy_1} + \\
&\quad\quad J_{z_1} \dot{\omega}_{gz_1} + (m_2 + m_3) \cdot \\
&\cdot l_g \left[\dot{V}_{gy_2} + \left(\dot{V}_{gy_1} + l_g \dot{\omega}_{gz_1} \right) \cos \vartheta_g + V_{gx_2} \omega_{gx_1} \sin \vartheta_g + \right. \\
&- (V_{gy_1} + \omega_{gz_1} l_g) \dot{\vartheta}_g \sin \vartheta_g - V_{gz_2} \omega_{gx_1} (\cos \vartheta_g + 1) + \\
&+ (V_{gy_1} \omega_{gy_2} - V_{gy_2} \omega_{gy_1}) \sin \vartheta_g + \\
&\left. + V_{gx_1} (\omega_{gz_1} + \omega_{gz_2}) \right] = M_c - M_{rc},
\end{aligned}
\tag{2}
$$

where

$$
\begin{aligned}
M_g &= (m_2 + m_3) \cdot l_g \cdot g \cdot cо\vartheta_g; \\
\dot{V}_{gx_1} &= \dot{V}_p \cos \psi_g - V_p \dot{\psi}_g \sin \psi_g; \\
\dot{V}_{gy_1} &= -\dot{V}_p \sin \psi_g - V_p \dot{\psi}_g \cos \psi_g; \\
\dot{V}_{gy_2} &= -\dot{V}_p \sin \psi_g - V_p \dot{\psi}_g \cos \psi_g + l_g (\dot{\omega}_{gz_1} + \dot{\omega}_{gz_2}); \\
\dot{\omega}_{gz_1} &= \left(\ddot{\psi}_g + \dot{r}^* \right); \\
\dot{\omega}_{gz_2} &= \dot{\omega}_{gx_1} \sin \vartheta_g + \omega_{gx_1} \dot{\vartheta}_g \cos \vartheta_g + \\
&\quad\quad + \dot{\omega}_{gz_1} \cos \vartheta_g - \omega_{gz_1} \dot{\vartheta}_g \sin \vartheta_g; \\
\dot{\omega}_{gx_1} &= \dot{p}^* \cos \psi_g - p^* \dot{\psi}_g \sin \psi_g + \dot{q}^* \sin \psi_g + q^* \dot{\psi}_g \cos \psi_g; \\
\dot{\omega}_{gx_2} &= \dot{\omega}_{gx_1} \cos \vartheta_g - \omega_{gx_1} \dot{\vartheta}_g \sin \vartheta_g - \\
&\quad\quad - \dot{\omega}_{gz_1} \sin \vartheta_g - \omega_{gz_1} \dot{\vartheta}_g \sin \vartheta_g; \\
\dot{\omega}_{gy_1} &= -\dot{p}^* \sin \psi_g - p^* \dot{\psi}_g \cos \psi_g + \dot{q}^* \cos \psi_g - q^* \dot{\psi}_g \sin \psi_g;
\end{aligned}
$$

$$
\begin{bmatrix} \omega_{gx_1} \\ \omega_{gy_1} \\ \omega_{gz_1} \end{bmatrix} = \begin{bmatrix} p^* \cos \psi_g + q^* \sin \psi_g \\ -p^* \sin \psi_g + q^* \cos \psi_g \\ \dot{\psi}_g + r^* \end{bmatrix};
$$

$$
\begin{bmatrix} \omega_{gx_2} \\ \omega_{gy_2} \\ \omega_{gz_2} \end{bmatrix} =
$$

$$
= \begin{bmatrix} (p^* \cos \psi_g + q^* \sin \psi_g) \cos \vartheta_g - \left(r^* + \dot{\psi}_g \right) \sin \vartheta_g \\ -p^* \sin \psi_g + q^* \cos \psi_g + \dot{\vartheta}_g \\ (p^* \cos \psi_g + q^* \sin \psi_g) \sin \vartheta_g + \left(r^* + \dot{\psi}_g \right) \cos \vartheta_g \end{bmatrix};
$$

$$
\begin{bmatrix} \omega_{gx_3} \\ \omega_{gy_3} \\ \omega_{gz_3} \end{bmatrix} =
$$

$$
= \begin{bmatrix} (p^* \cos \psi_g + q^* \sin \psi_g) \cos \vartheta_g - \left(r^* + \dot{\psi}_g \right) \sin \vartheta_g + \dot{\Phi}_g \\ -p^* \sin \psi_g + q^* \cos \psi_g + \dot{\vartheta}_g \\ (p^* \cos \psi_g + q^* \sin \psi_g) \sin \vartheta_g + \left(r^* + \dot{\psi}_g \right) \cos \vartheta_g \end{bmatrix};
$$

$$
\begin{aligned}
V_{gx_2} &= V_p \cos \vartheta_g \cos \psi_g + l_g \omega_{gy_1} \sin \vartheta_g; \\
V_{gy_2} &= -V_p \sin \psi_g + l_g (\omega_{gz_1} + \omega_{gz_2}); \\
V_{gz_2} &= V_p \sin \vartheta_g \cos \psi_g - l_g (\omega_{gy_1} \cos \vartheta_g + \omega_{gy_2}); \\
V_{gx_1} &= V_p \cos \psi_g; \\
V_{gy_1} &= -V_p \sin \psi_g; \\
V_{gz_1} &= 0.
\end{aligned}
$$

Basing on the equations of motion derived for the launcher-missile-gyroscope system presented in [2], it was possible to perform a numerical analysis of the behavior of a self-propelled anti-aircraft missile system during the motion over uneven terrain. It should be emphasized that the system effectiveness is largely dependent on the accuracy of the gyroscope, which constitutes the control drive of the head of the tracking missile, i.e. the target coordinator. Thermal radiation falls on the infrared detector through the lens and the raster. The detector converts them into an electric signal [3], which contains information about the direction and magnitude of the angular displacement between the position of the line of sight in space and the optical axis of the lens. The signal parameters, such as frequency or phase, are related to the position of the dot on the raster, i.e. the position of the target in space. The signal is transmitted from the detector to the electronic unit. This desired signal and the one resulting from the position of the gyroscope axis in space determine the deviation of the gyroscope control system. It is necessary to conduct a comprehensive study concerning the effects of the kinematic excitations generated by the motions of the launcher and the missile on the gyroscope performance. We consider the variation in the angular velocity $\overrightarrow{\omega}_p (p^*, q^*, r^*)$ defined by the following equations:

$$
\begin{aligned}
p^* &= \dot{\varphi}_v \cos \vartheta_{pv} \cos \psi_{pv} - \dot{\vartheta}_v \cos \vartheta_{pv} \sin \psi_{pv}, \\
q^* &= \dot{\vartheta}_v \sin \vartheta_{pv} \sin \psi_{pv} - \dot{\varphi}_v \sin \vartheta_{pv} \cos \psi_{pv}, \\
r^* &= \dot{\vartheta}_v \cos \psi_{pv} + \dot{\varphi}_v \sin \psi_{pv}
\end{aligned}
\tag{3}
$$

and the variation in the linear velocity $\overrightarrow{V}_p \left(V_{px_v}, V_{py_v}, V_{pz_v}\right)$ of the missile motion along the launcher [4] described by the following equations:

$$V_{px_v} = \left(l_\xi - l_\eta \vartheta_v\right) \dot{\xi}_{pv} - l_\eta \xi_{pv} \dot{\vartheta}_v,$$
$$V_{py_v} = \left(l_\eta + l_\xi \vartheta_v - l_\zeta \varphi_v\right) \dot{\xi}_{pv} + l_\xi \xi_{pv} \dot{\vartheta}_v - l_\zeta \xi_{pv} \dot{\varphi}_v + \dot{y}_v,$$
$$V_{pz_v} = \left(l_\zeta + l_\eta \varphi_v\right) \dot{\xi}_p + l_\eta \xi_{pv} \dot{\varphi}_v. \tag{4}$$

All the quantities in Eqs. (3) and (4) were described in [2]. The kinematic interactions can cause disturbances of the gyroscope motion, which are due to the inevitable friction in the bearings of the gyroscope frames and the non-concentricity of the mass centre and the rotation centre.

2. Kinematic excitations

2.1. Excitations affecting the launcher performance. The analysis concerned the behavior of a launcher mounted on a wheeled vehicle going over a single bump with the front and rear wheels [4]. It was assumed that the basic motion of the vehicle carrying the launcher can be described from the formula $s_n = V_n \cdot (t - t_{gb})$, where: $V_n = 8.3$ m/s – velocity of the vehicle with the launcher; $t_{gb} = 0.5$ s – time in which the vehicle carrying the launcher climbs a bump with the front wheels. The form of the excitations were modeled by applying the following equations:

$$y_{01} = y_0 \sin^2 \left(\omega_0 \cdot s_n\right),$$
$$\dot{y}_{01} = y_0 \omega_0 V_n \sin \left(2\omega_0 \cdot s_n\right), \tag{5a}$$

$$y_{02} = y_0 \sin^2 \left(\omega_0 \cdot s_n\right),$$
$$\dot{y}_{02} = y_0 \omega_0 V_n \sin \left(2\omega_0 \cdot s_n\right), \tag{5b}$$

$$y_{03} = y_0 \sin^2 \left[\omega_0 \left(s_n - l_{wn}\right)\right],$$
$$\dot{y}_{03} = y_0 \omega_0 V_n \sin \left[2\omega_0 \left(s_n - l_{wn}\right)\right], \tag{5c}$$

$$y_{04} = y_0 \sin^2 \left[\omega_0 \left(s_n - l_{wn}\right)\right],$$
$$\dot{y}_{04} = y_0 \omega_0 V_n \sin \left[2\omega_0 \left(s_n - l_{wn}\right)\right], \tag{5d}$$

where $y_0 = 0.05$ m, $l_0 = 0.35$ m, $\omega_0 = \dfrac{\pi}{l_0}$, $l_{wn} = l_1 + l_2$.

2.2. Excitations affecting the gyroscope performance. If we assume that the gyroscope performs small motions round its position of equilibrium, then the moments of the viscous friction forces in the bearings of the gyroscope frames can be approximately written as [1]:

$$M_{rb} = \eta_b \cdot q^* = \eta_b \left(\dot{\vartheta}_v \sin \vartheta_{pv} \sin \psi_{pv} - \dot{\varphi}_v \sin \vartheta_{pv} \cos \psi_{pv}\right), \tag{6a}$$

$$M_{rc} = \eta_c \cdot r^* = \eta_c \left(\dot{\vartheta}_v \cos \psi_{pv} + \dot{\varphi}_v \sin \psi_{pv}\right) \tag{6b}$$

where η_b, η_c – coefficients of the moments of the viscous friction forces.

Equations (6) show that the kinematic excitation of the launcher causes an excitation of the gyroscope through friction

in the bearings of the frames. It is not possible to completely eliminate the friction, thus a rapid motion of the launcher will have influence on the accuracy of the pre-determined position of the gyroscope axis in space. The higher the values of coefficients η_b and η_c, the more visible the drifts of the gyroscope axis will be. To prevent this undesirable phenomenon, it is necessary to apply additional correction moments to the gyroscope frames [1]:

$$M_b = -k_b \vartheta_g + k_c \psi_g - h_g \frac{d\vartheta_g}{dt} \tag{7a}$$

$$M_c = -k_c \vartheta_g - k_b \psi_g - h_g \frac{d\psi_g}{dt} \tag{7b}$$

where k_b, k_c – coefficients of the corrector amplifications; h_g – coefficient of the corrector attenuation.

3. Results

The effect of the launcher motion on the gyroscope performance was analyzed using a hypothetical anti-aircraft system with short-range missiles, which was described in Ref. [2]. The following parameters were assumed for the gyroscope:

$$J_{x_1} = 2.5 \cdot 10^{-5} \text{ kgm}^2, \quad J_{y_1} = J_{x_1},$$
$$J_{z_1} = J_{x_1}, \quad J_{x_2} = 5 \cdot 10^{-5} \text{ kgm}^2,$$
$$J_{y_2} = J_{x_2}, \quad J_{z_2} = J_{x_2},$$
$$J_{x_3} = 5 \cdot 10^{-4} \text{ kgm}^2,$$
$$J_{y_3} = J_{x_3}, \quad J_{z_3} = J_{x_3},$$
$$m_2 = 0.1 \text{ kg}, \quad m_3 = 0.14 \text{ kg},$$
$$m = m_2 + m_3, \quad n_g = 500 \text{ rad/s},$$
$$l_g = 0.002 \text{ m}, \quad \eta_b = \eta_b = 0.01 \text{ Nms};$$
$$k_b = 31.5, \quad k_c = -3, \quad h_g = 31.5.$$

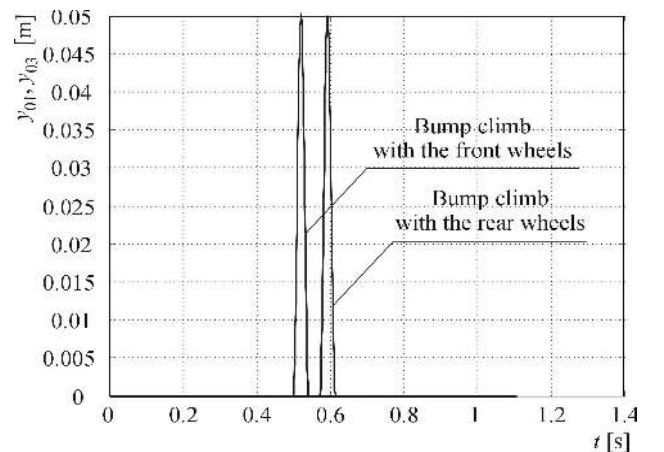Selected results of the computer simulation are presented in Figs. 2–13.

Fig. 2. A profile of a single obstacle (bump) in the function of time
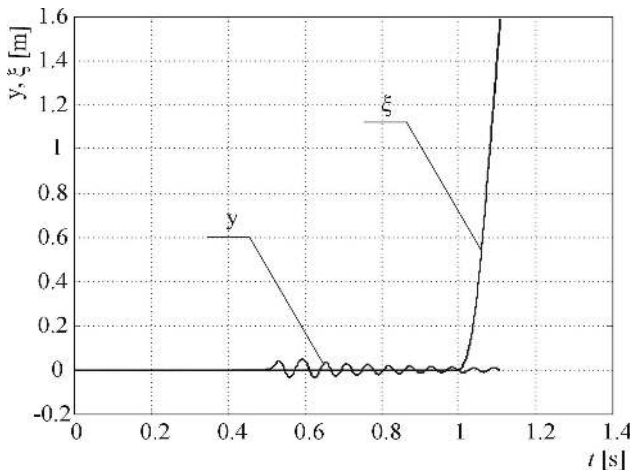
Fig. 3. Vertical displacements of the launcher and progressive displacements of the missile with regard to the guide rail in the function of time
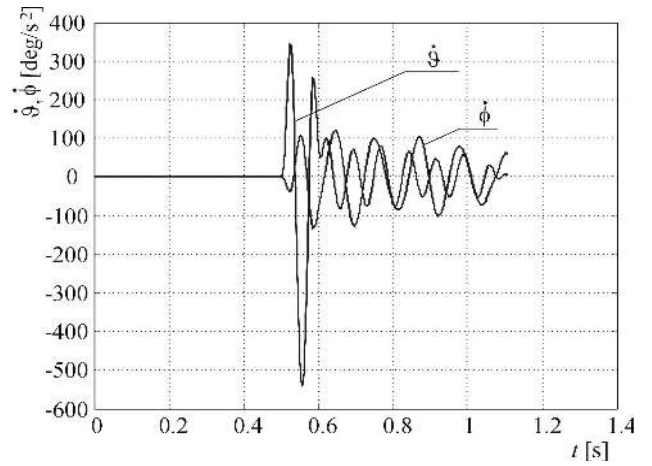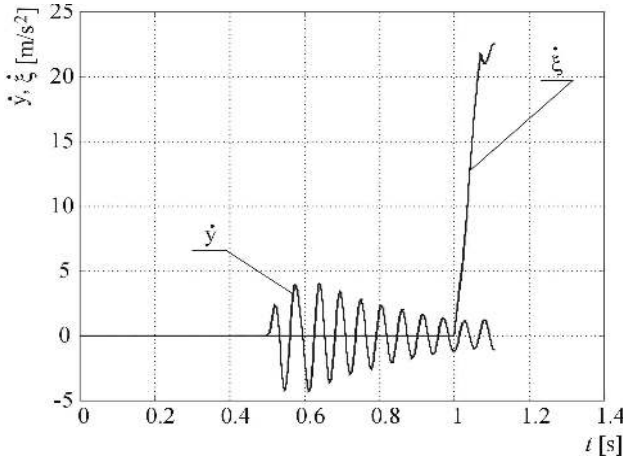

Fig. 4. Velocities of the vertical displacements of the launcher and progressive displacements of the missile with regard to the guide rail in the function of time
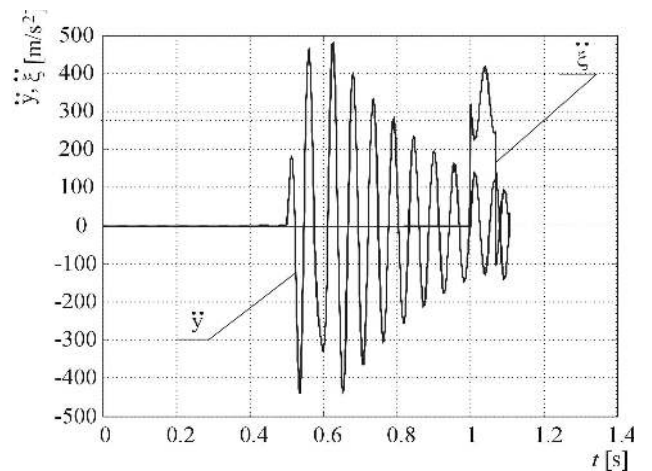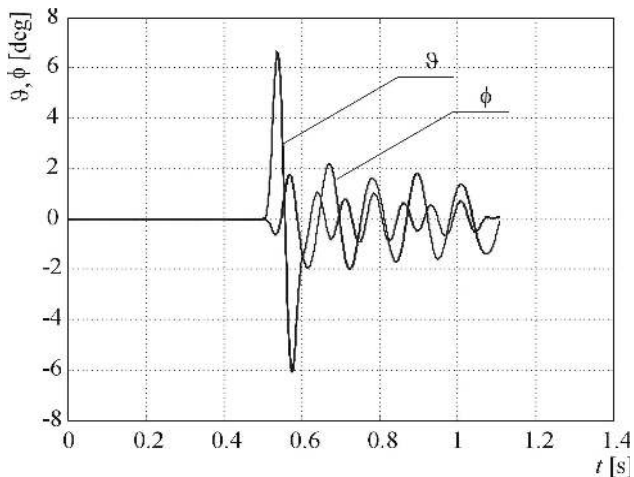

Fig. 5. Angular displacements of the launcher in the function of time

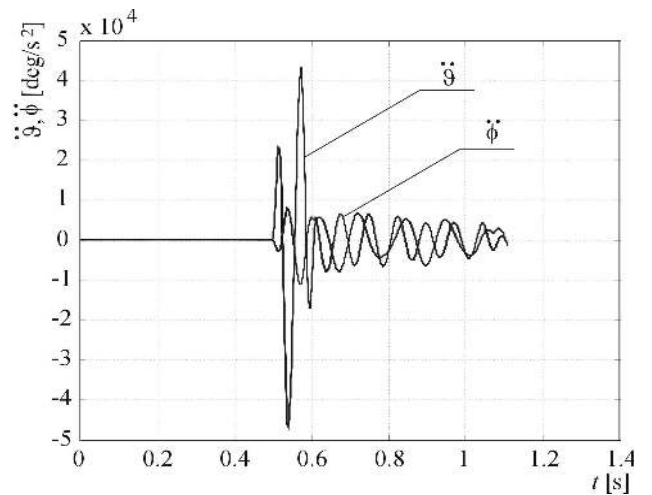

Fig. 6. Angular velocities of the launcher in the function of time

Fig. 7. Vertical accelerations of the launcher and progressive accelerations of the missile with regard to the guide rail in the function of time

Fig. 8. Angular accelerations of the launcher in the function of time
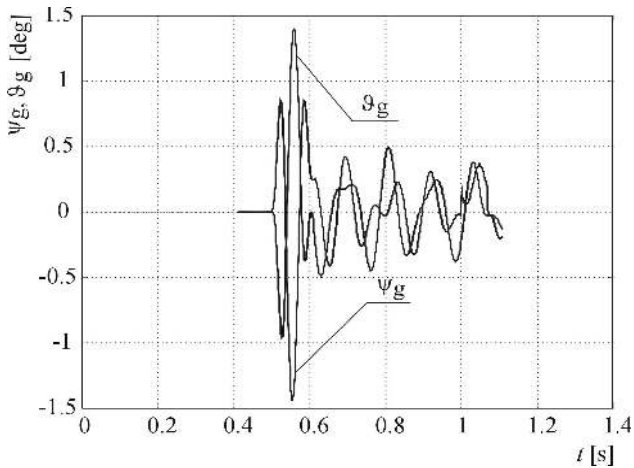
Fig. 9. Angular displacements of the gyroscope axis in the function of time without correction
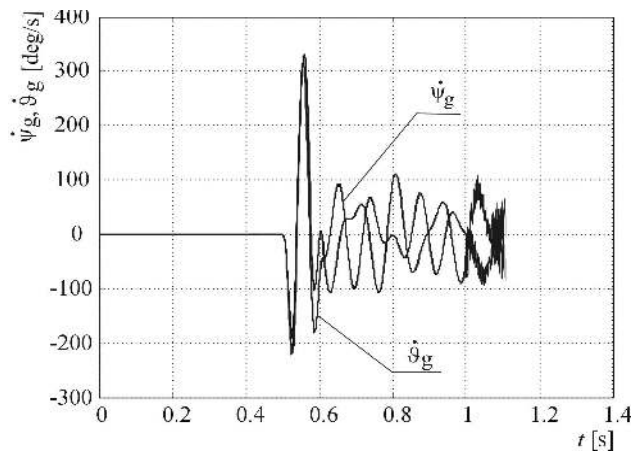

Fig. 10. Angular velocities of the gyroscope axis in the function of time without correction
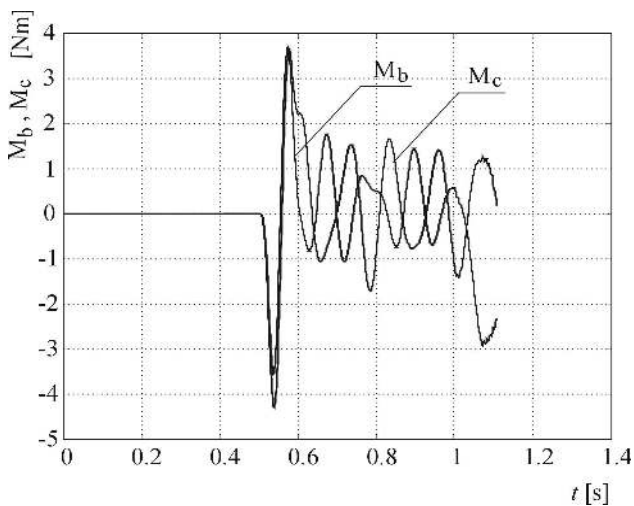

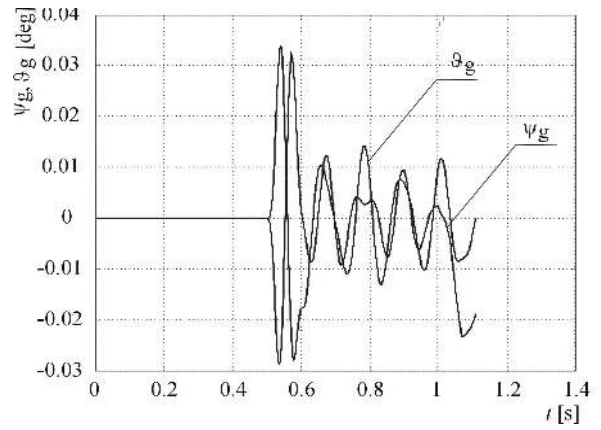Fig. 11. Corrective control moments of the gyroscope in the function of time

Fig. 12. Angular displacements of the gyroscope axis in the function of time with correction
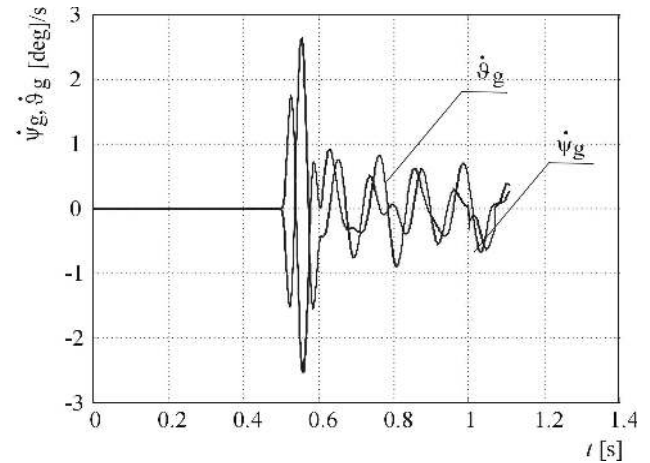

Fig. 13. Angular velocities of the gyroscope axis in the function of time with correction

4. Conclusions

The results of the computer simulation show that maintaining the gyroscope axis in the pre-determined position during target tracking is difficult when the vehicle is climbing a bump and when the missile is moving along the guide rail, as shown in Figs. 9 and 10. A displacement of the gyroscope axis from the pre-determined position by several steps can lead to the loss of the target image in the field of view of the target coordinator lens. These additional displacements of the gyroscope axis need to be minimized by the automated correction system described by Eq. (7). The displacements – whether big or small – always appear during the gyroscope operation, no matter how advanced the technology applied is. The gyroscope becomes more resistant to undesirable kinematic interaction of the launcher and the missile motion along the guide rail (Figs. 12 and 13) after correction controls M_b and M_c are applied (Fig. 11). The results confirm the suitability of the algorithm used to correct the gyroscope operation affected by disturbances generated by the launcher and the missile.

REFERENCES

[1] Z. Koruba, "Dynamics and control of a gyroscope on board of an flying object", in *Monographs, Studies, Dissertations*, vol. 25, Kielce University of Technology, Kielce, 2001, (in Polish).

[2] Z. Dziopa, Z. Koruba, and I. Krzysztofik, " An analysis of the dynamics of a launcher-missile system on a moveable base", in *Monographs, Studies, Dissertations*, vol. 34, Kielce University of Technology, Kielce, 2010, (in Polish).

[3] I. Krzysztofik and J. Osiecki, *Detection and Tracking of Targets*, Scientific Issue of Kielce University of Technology, vol. 32, No. 430, Kielce, 2008.

[4] Z. Dziopa, "The modelling and investigation of the dynamic properties of the sel-propelled anti-aircraft system, *Monographs, Studies, Dissertations* vol. 32, No. M9, Kielce University of Technology, Kielce, 2008.

[5] V.P. Mishin, *Missile Dynamics*, Mashinostroyeniye, Moscow, 1990.

[6] V.A. Svietlitskiy, *Dynamics Start Flying Objects*, Nauka, Moscow, 1963.